

Continuous isolated noise sources induce repeating waves in the coda of ambient noise correlations

S. Schippkus *, M. Safarkhani ¹, C. Hadziioannou ¹

¹Institute of Geophysics, Centre for Earth System Research and Sustainability (CEN), Universität Hamburg, Hamburg, Germany

Author contributions: *Conceptualization*: SS, MS, CH. *Methodology*: SS. *Software*: SS. *Data curation*: MS. *Formal Analysis*: SS. *Investigation*: SS, MS.

Resources: SS, CH. *Writing - original draft*: SS. *Writing - Review & Editing*: tbd. *Visualization*: SS. *Supervision*: CH. *Funding acquisition*: SS, CH.

Abstract Continuous excitation of isolated noise sources leads to repeating wave arrivals in cross correlations of ambient seismic noise, including throughout their coda. These waves propagate from the isolated sources. We observe this effect on correlation wavefields computed from two years of field data recorded at the Gräfenberg array in Germany and two master stations in Europe. Beamforming the correlation functions in the secondary microseism frequency band reveals repeating waves incoming from distinct directions to the West, which correspond to well-known dominant microseism source locations in the Northeastern Atlantic Ocean. These emerge in addition to the expected acausal and causal correlation wavefield contributions by boundary sources, which are converging onto and diverging from the master station, respectively. Numerical simulations reproduce this observation. We first model a source repeatedly exciting a wavelet, which helps illustrate the fundamental mechanism behind repeated wave generation. Second, we model continuously acting secondary microseism sources and find good agreement with our observations. Our observations and modelling have potentially significant implications for the understanding of correlation wavefields and monitoring of relative velocity changes in particular. Velocity monitoring commonly assumes that only multiply scattered waves, originating from the master station, are present in the coda of the correlation wavefield. We show that repeating waves propagating from isolated noise sources may dominate instead, including the very late coda. Our results imply that in the presence of continuously acting noise sources, which we show is the case for ordinary recordings of ocean microseisms, velocity monitoring assuming scattered waves may be adversely affected with regard to measurement technique, spatial resolution, as well as temporal resolution. We further demonstrate that the very late coda of correlation functions contains useful signal, contrary to the common sentiment that it is dominated by instrument noise.

Non-technical summary Seismic waves are generated by all kinds of sources, including earthquakes, ocean waves, and machinery. Some sources produce a consistently present background level of seismic energy, so-called ambient seismic noise. It is well-established that, under

*Corresponding author: sven.schippkus@uni-hamburg.de

34 the condition of evenly distributed noise sources, cross-correlation of ambient seismic noise, which
35 was recorded on two separate seismic stations, yields a new wavefield that propagates directly
36 from one station to the other. We call this new wavefield the correlation wavefield. Here, we show
37 that in the presence of an additional isolated noise source that excites seismic waves continuously,
38 for example ocean waves induced by storm systems over the Northeastern Atlantic, a new contri-
39 bution to the correlation wavefield emerges: repeating waves propagating from the isolated noise
40 source. These repeating waves can be more coherent across several stations than the expected
41 correlation wavefield contribution, which propagates from one station to the other. We observe
42 such repeating waves propagating from isolated noise sources on correlation wavefields computed
43 from two years of seismic recordings of the Gräfenberg seismic array in Germany and two master
44 stations in Europe. We reproduce our observations with numerical simulations of the sources and
45 resulting correlation wavefields. Our findings have potentially significant implications for seismic
46 monitoring based on relative velocity changes, which is used to monitor geological faults, volca-
47 noes, groundwater, and other processes in the Earth. Velocity monitoring commonly relies on the
48 assumption that the correlation wavefield contains only the contribution that propagates from one
49 station to the other, which we show is not necessarily correct. This can lead to misinterpretation of
50 measured velocity variations.

51 **1 Introduction**

52 Seismic interferometry of the ambient seismic field gives rise to new correlation wavefields that relate to the Green's
53 function under the condition of uniformly distributed noise sources (Wapenaar et al., 2005; Gouédard et al., 2008).
54 These correlation wavefields are now routinely used for imaging (e.g., Schippkus et al., 2018; Lu et al., 2018) and mon-
55 itoring (e.g., Wegler and Sens-Schönfelder, 2007; Hadziioannou et al., 2009; Sheng et al., 2023) of Earth's structure. In
56 the presence of an isolated noise source, a second contribution to this wavefield is introduced, sometimes referred
57 to as spurious arrival (Snieder et al., 2006; Zeng and Ni, 2010; Retailleau et al., 2017; Schippkus et al., 2022). This cor-
58 relation wavefield contribution can lead to biased measurements of seismic wave speed due to interference of direct
59 waves from the master station and the isolated noise source (Schippkus et al., 2022).

60 Monitoring applications, on the other hand, rely on estimating relative velocity changes by repeatedly computing
61 correlation wavefields throughout time and measuring changes in the arrival time of their coda (Wegler and Sens-
62 Schönfelder, 2007; Sens-Schönfelder and Larose, 2010). Current strategies often rely on the assumption that the
63 coda of a given correlation wavefield is comprised of multiply scattered waves, originating from the master station,
64 which also dictates its spatial sensitivity (Planès et al., 2014; Margerin et al., 2016; van Dinter et al., 2021). If the
65 spatial sensitivity of the coda is known, seismic velocity changes can be located (Obermann et al., 2014; Mao et al.,
66 2022). Some progress has been made in accounting for the impact of changes in sources on the correlation wavefield,
67 particularly in the context of monitoring at frequencies above 1 Hz, e.g., by carefully selecting time windows in which
68 the same sources are active and produce similar correlation wavefields (Yates et al., 2022; Sheng et al., 2023).

69 In this study we demonstrate that isolated noise sources may impact correlation wavefields to a degree previously
 70 not considered. Continuously acting isolated noise sources, such as ocean microseisms, produce repeating waves
 71 throughout the entire correlation function that propagate from the isolated source location. These waves coincide
 72 with and are more coherent than multiply scattered waves originating from the master station. This may have sig-
 73 nificant impact on the understanding of measured velocity changes. In the following, we show observations of these
 74 repeating waves on field data correlation functions in the ocean microseism frequency band using stations through-
 75 out Europe, illustrate the mechanism behind repeated direct-wave generation in correlation functions, and finally
 76 reproduce our field data observations by modelling continuously acting isolated noise sources, i.e., secondary ocean
 77 microseisms.

78 2 Beamforming the correlation wavefield

79 We compute correlation wavefields from two years of continuous vertical component seismograms, recorded in 2019
 80 and 2020 at the Gräfenberg array in Germany and two master stations, IV.BRMO in Italy (Fig. 1a) and PL.OJC in Poland
 81 (Fig. 2a). We apply a standard processing workflow: remove instrument response, cut two years of data into two-hour
 82 long segments overlapping by 50%, apply spectral whitening (Bensen et al., 2007), cross-correlate each segment, and
 83 stack all segments linearly. No further processing, e.g., earthquake removal or other segment selection, has been
 84 applied.

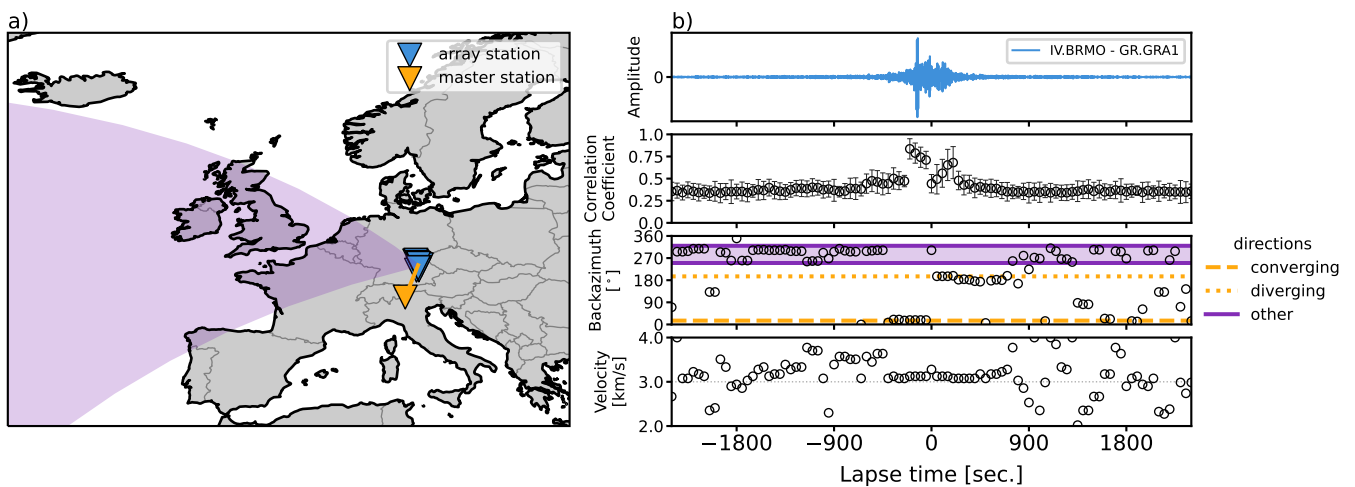


Figure 1 Beamforming the correlation wavefield between the Gräfenberg array in Germany (blue triangle) and master station IV.BRMO, Italy (yellow triangle), in the secondary microseism frequency band (0.1 to 0.3 Hz). a) Overview map with master station and array stations. The orange line and purple area correspond to the dominant directions detected by beamforming. b) Beamforming results: sample cross-correlation between the master station and one array station (top), mean Pearson correlation-coefficient of correlation functions with best-fitting beams in each window (second panel), detected direction of arrival (third panel), and estimated phase velocity (bottom). Detected directions correspond to the correlation wavefield converging onto and diverging from the master station (orange lines), and a range of directions pointing towards the Atlantic Ocean (purple area).

85 To estimate from which directions the correlation wavefield arrives at the Gräfenberg array, we beamform the
 86 correlation functions (Fig. 1). We beamform in 200 sec. windows, overlapping by 75%, in the secondary micro-
 87 seism frequency band (0.1 to 0.3 Hz), and assuming plane-wave propagation (Rost and Thomas, 2002). We present a
 88 sample correlation function to give orientation in lapse time (Fig. 1b, top panel), and compute Pearson correlation
 89 coefficients of all correlation functions with the best-fitting beam for each window to estimate how well the beam ex-

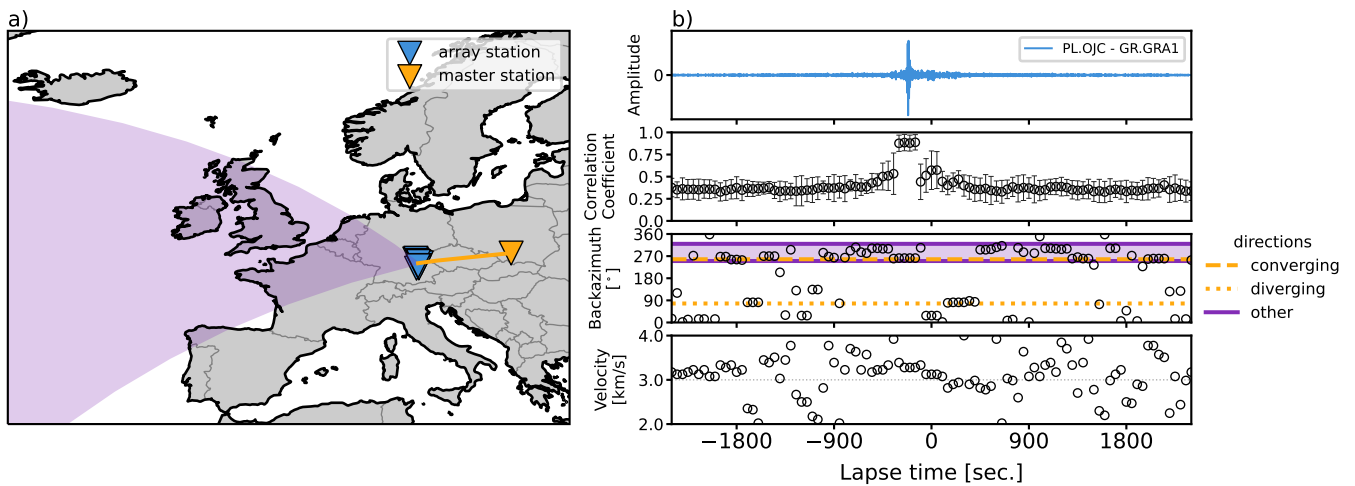


Figure 2 Same as Figure 1, but for master station PL.OJC, Poland. The directions detected by beamforming corresponding to the diverging and converging part of the correlation wavefield change with master station as expected (orange lines), whereas the range of directions towards the Northern Atlantic remains constant (purple area). Note that the converging part of the correlation wavefield points towards West, similar to one of the dominant directions detected pointing towards the Atlantic Ocean for master station IV.BRMO (Fig. 1).

90 plains the data within a window (Fig. 1b, second panel). Similarity is highest for the expected acausal arrival, which
 91 also emerges more clearly in the correlation function than the causal arrival, due to the commonly observed strong
 92 noise sources in the Northeastern Atlantic (e.g., Friedrich et al., 1998; Chevrot et al., 2007; Juretzek and Hadziioan-
 93 nou, 2016). Throughout the coda, similarity remains nearly constant with a correlation coefficient ~ 0.4 . We detect
 94 several dominant directions of arrival (Fig. 1b, third panel). First, the acausal arrival of the correlation wavefield
 95 converging onto the master station at negative lapse time (dashed orange line) and the causal arrival diverging from
 96 the master station at positive lapse time (dotted orange line), i.e., the correlation wavefield contribution that usu-
 97 ally arises in seismic interferometry (Wapenaar et al., 2005). Second, distinct directions throughout the correlation
 98 functions pointing towards West (Fig. 1b, third panel), which we project onto the map view (Fig. 1a).

99 A second master station in Poland (PL.OJC) illustrates how the converging (acausal) and diverging (causal) parts
 100 of the correlation wavefield depend on the geometry of array stations to master station and point roughly towards
 101 the great-circle between the two (Soergel et al., 2022), whereas the dominant directions towards West appear to be
 102 independent of the master station (Fig. 2). A North-Northeast direction, however, still emerges in the beamforming
 103 results as most coherent, which coincides approximately with the great circle direction for the converging part of
 104 the correlation wavefield for master station IV.BRMO (Fig. 1). Similarly, the converging direction for master station
 105 PL.OJC coincides with the dominant directions towards West (Fig. 2). This hints at the impact the geometry of master
 106 station and array stations has on the detection and identification potential of these other directions. We propose the
 107 dominant directions detected by beamforming and pointing towards West represent repeating direct waves emerg-
 108 ing at isolated noise source locations in the Northeastern Atlantic Ocean. We call these direct waves, because they
 109 propagate directly from the isolated source to the seismic stations. These are not to be confused with the direct waves
 110 propagating between the stations, i.e., the expected acausal and causal arrivals.

3 A repeating impulsive isolated noise source

To substantiate our hypothesis and explain the observations above, we start from the concept of an isolated noise source (Schippkus et al., 2022). Consider a wavefield that is excited by sources on a boundary S and an isolated noise source at \mathbf{r}_N , recorded on a station at location \mathbf{r}

$$u(\mathbf{r}) = \oint_S N_B(\mathbf{r}')G(\mathbf{r}, \mathbf{r}')d\mathbf{r}' + N_I G(\mathbf{r}, \mathbf{r}_N), \quad (1)$$

with G the Green's function and N_B and N_I the source spectra of boundary sources and the isolated source, respectively. This section is formulated in the frequency domain. The cross-correlation of this wavefield at location \mathbf{r} with the wavefield recorded on a master station at \mathbf{r}_M is given by (eq. 6 of Schippkus et al., 2022)

$$\langle u(\mathbf{r})u^*(\mathbf{r}_M) \rangle = \frac{\rho c |N_B|^2}{2} (G(\mathbf{r}, \mathbf{r}_M) + G^*(\mathbf{r}, \mathbf{r}_M)) + |N_I|^2 G(\mathbf{r}, \mathbf{r}_N)G^*(\mathbf{r}_M, \mathbf{r}_N), \quad (2)$$

where the first term describes the contribution of uncorrelated sources on the boundary S surrounding the stations (as in Wapenaar et al., 2005), which usually arises in seismic interferometry, and the second term describes the contribution of the isolated noise source. The relation of these terms has been investigated by Schippkus et al. (2022), who demonstrate how the direct arrivals of these two wavefield contributions interfere for certain station geometries, leading to biased surface wave dispersion measurements. In their modelling, the authors assumed the source term of the isolated source N_I to be a wavelet, excited once.

Here, we expand upon this idea by considering the isolated noise source to be excited multiple times in a correlated manner. For illustration purposes, we express its source term as $N_I = W_I E_I$, with a wavelet W_I and excitation pattern E_I . The contribution of the isolated noise source to the correlation wavefield is hence

$$|W_I|^2 |E_I|^2 G(\mathbf{r}, \mathbf{r}_N)G^*(\mathbf{r}_M, \mathbf{r}_N). \quad (3)$$

A simple example of an isolated noise source exciting a Ricker wavelet, repeating 5 times with a 20 sec. interval, illustrates how such a source manifests in correlation functions (Fig. 3). For such a source, the excitation pattern is a time series with 1 at every interval of 20 sec. (5 times), and 0 elsewhere. The auto-correlation of the wavelet $|W_I|^2$ (Fig. 3a), auto-correlation of the excitation pattern $|E_I|^2$ (Fig. 3b), and cross-correlation of the Green's functions $G(\mathbf{r}, \mathbf{r}_N)G^*(\mathbf{r}_M, \mathbf{r}_N)$ for surface waves in a homogeneous, isotropic, acoustic medium and an arbitrary geometry (Fig. 3c) are convolved to result in a repeating wavelet with the same 20 sec. interval, present in the correlation wavefield (Fig. 3d). These repeating wavelets represent direct waves emitted from the isolated source location.

A sketch of the correlation wavefield in the presence of a repeating impulsive isolated noise source helps illustrate its evolution with lapse time (Fig. 4). The wavefield is comprised of the two contributions by boundary sources (first term of eq. 2, yellow in Fig. 4) and the isolated noise source (eq. 3, purple in Fig. 4). The boundary source contribution converges onto the master station at negative lapse times (the acausal part), and diverges from the station at positive lapse times (the causal part, Fig. 4a-g). This is the expected contribution that usually arises in seismic interferometry. The repeating isolated noise source induces waves that emerge earlier and with lower amplitude than the main arrival

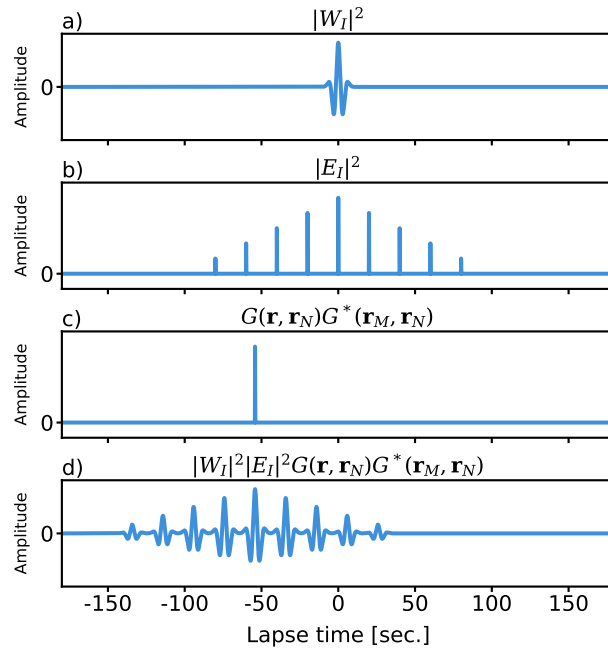


Figure 3 A repeating isolated noise source produces repeating direct waves in correlation functions, depicted in time domain. a) Auto-correlation of the wavelet $|W_I|^2$. b) Auto-correlation of the excitation pattern $|E_I|^2$ with a regular 20 sec. interval, excited 5 times. Note that amplitudes decay by $1/5$ every interval away from 0 sec. lapse time. c) Cross-correlation of the Green's functions between the isolated noise source and both station locations for an arbitrary geometry. d) Second term of the correlation wavefield (eq. 3, the convolution of a-c), where each arriving wavelet represents a direct wave emitted from the isolated noise source at \mathbf{r}_N .

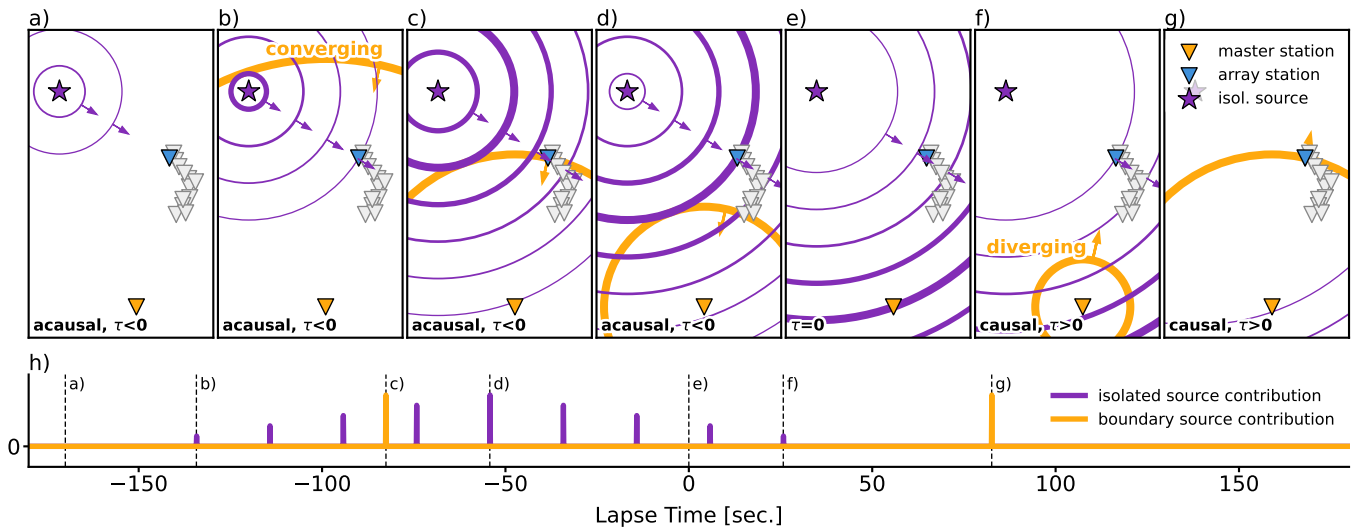


Figure 4 Schematic illustration of the correlation wavefield in the presence of a repeating impulsive source (5 excitations, 20 sec. interval, same as in Figure 3). We remove the wavelet for improved clarity. a-g) Snapshots of the correlation wavefield at different lapse times, indicated by dashed lines in h). The contributions of the isolated source (purple lines) and boundary sources surrounding the master and array stations (yellow line) propagate through the medium. Line thickness indicates amplitude. h) Correlation function between the array station and the master station, color-coded by isolated source and boundary source contribution (purple and yellow, respectively). Dashed vertical lines mark the lapse time snapshots displayed in a-g). The acausal part of the correlation function contains repeating waves propagating from the isolated source and the boundary source contribution converging onto the master station (a-d). At lapse time $\tau = 0$, both the main arrival of the isolated source contribution and the boundary source contribution reach the master station (e). At causal lapse time, the last arrivals of the isolated source reach the array station (f) and finally the diverging contribution of the boundary sources (g).

(Fig. 4a) and eventually reach the array station (4b). The main arrival (highest amplitude, indicated by line thickness) of the isolated noise source emerges at $\tau = -|\mathbf{r}_M - \mathbf{r}_N|/c$ and touches the boundary source contribution along the line connecting the isolated source and master station (c-f, as in Schippkus et al., 2022). At lapse time $\tau = 0$, both the wavefield contribution by boundary sources and the main arrival of the isolated noise source reach the master station (Fig. 4e). At causal lapse times, the last repeating waves from the isolated noise source reach the array station (Fig. 4f) before the boundary source contribution diverging from the master station arrives at the array station (Fig. 4g). The exact timing of each arrival depends on the geometry of isolated source, master station, and array stations, as well as the excitation pattern.

Note that the repeating direct waves from the isolated noise source are asymmetrical in lapse time (Figs. 3, 4), because there is no part of the correlation wavefield converging onto the isolated noise source (Schippkus et al., 2022). How strongly these repeating direct waves manifest depends on how highly correlated the isolated source is with itself throughout time. The example presented here constitutes the most extreme case, i.e., identical wavelet and exactly regular excitation pattern. Even under these conditions, amplitudes decay linearly with time due to the finite length of the excitation pattern (Fig. 3b). In this example, the amplitude of the excitation pattern auto-correlation decreases by 1/5 of the maximum amplitude with each interval away from 0 sec., because the source is excited 5 times. Slight variations in amplitude, shape of the wavelet, or excitation timing lead to reduced correlation, and thus repeating direct waves with reduced amplitude or different shape. If there was no correlation, they would disappear.

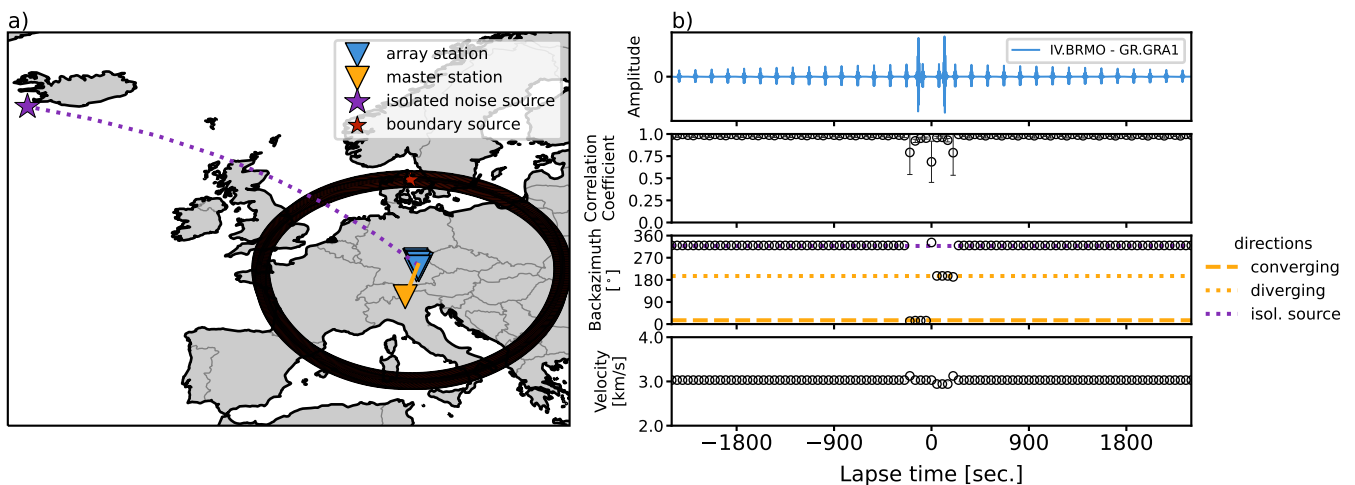


Figure 5 Beamforming synthetic cross-correlation functions detects repeating direct waves from the regularly repeating isolated noise source. a) Overview map: master station (orange triangle), array stations (blue triangle), boundary sources in a small circle surrounding the stations (red stars) and the isolated noise source Southwest of Iceland (purple star). b) Beamforming results: sample cross-correlation between master station and one array station, mean correlation-coefficients between windowed correlation functions and beams, detected direction of arrival, and estimated phase velocity. The boundary source contribution to the correlation wavefield converging onto and diverging from the master station (orange lines, first term in eq. 2) is detected as well as repeating direct waves from the isolated noise source (purple line, second term in eq. 2).

To confirm the repeating wavelets in the correlation functions indeed represent repeating direct waves emitted from the isolated noise source, we model a master station in Italy (same location as IV.BRMO), array stations in Southern Germany (same locations as the Gräfenberg array), 1000 boundary sources surrounding the stations in a small-circle with 1000 km distance to them, as well as a repeating isolated noise source Southwest of Iceland (Fig. 5a). All sources excite Ricker wavelets, and only the isolated noise source repeats it 50 times with a 150 sec. inter-

162 val (similar to Figs. 3, 4). We compute synthetic surface wave seismograms by assuming a homogeneous, isotropic,
 163 acoustic half-space with a medium velocity $v = 3$ km/s for simplicity (i.e., Green's functions are of the form $e^{-i\omega x/v}$),
 164 and compute cross correlations of those waveforms. During the calculations, we treat boundary sources and the iso-
 165 lated noise source separately in accordance with equation (2). The maximum amplitude of the isolated noise source
 166 contribution is scaled to 1/4 of the boundary source contribution to distinguish them easily (Fig. 5b, top panel). The
 167 correlation wavefield contains both wavefield contributions. Beamforming the cross-correlation functions between
 168 the master station and all array stations detects three directions of arrival (Fig. 5b, third panel): the first term of
 169 the correlation wavefield converging onto the master station at negative lapse time (dashed orange line) and diverg-
 170 ing from the master station at positive lapse time (dotted orange line), and repeating direct waves from the isolated
 171 source (purple dotted line) throughout the correlation function. The estimated phase velocity of ~ 3 km/s is the
 172 medium velocity (Fig. 5b, bottom panel). Note that the correlation functions match exactly with the beam (correla-
 173 tion coefficient of 1) only for time windows that do not contain both contributions simultaneously (Fig. 5b, second
 174 panel).

175 This example illustrates the principle behind repeating direct waves emerging in correlation functions. However,
 176 we observed this effect on field data of secondary ocean microseisms (Figs. 1, 2), which are better described as
 177 continuously acting sources.

178 4 Continuously acting isolated noise sources

179 To describe the suspected isolated noise source (Figs. 1, 2) as a continuously acting microseism source, we rely on
 180 the parametrization employed by Gualtieri et al. (2020) (eq. 3 therein). The surface pressure P at colatitude θ and
 181 longitude ϕ excited by the secondary microseism mechanism is described as a superposition of many harmonics

$$182 P(t, \theta, \phi) = \sum_{i=1}^H A(f_i, \theta, \phi) \cos(2\pi f_i t + \Phi_i), \quad (4)$$

183 with H the number of harmonics, A the amplitude of the harmonic frequency f_i , and Φ_i its phase. The amplitude
 184 A relates to the power spectral density of ocean gravity waves and incorporates local site effects, and is described
 185 in more detail by Gualtieri et al. (2020). For our considerations, we neglect the amplitude term ($A = 1$), because
 186 we investigate a fairly narrow frequency band and the exact amplitude of each harmonic is irrelevant for explaining
 187 the effect observed in this study. In the following, we use $P(\theta, \phi)$ (the spectrum of $P(t, \theta, \phi)$) with harmonics from
 188 0.1 to 0.3 Hz directly as the source term N_I (Fig. 6a). Its auto-correlation (Fig. 6b), convolved with the same Green's
 189 function cross-correlation as above (Fig. 3c) contains one clear main arrival and weak, repeating direct waves (Fig.
 190 6c). These repeating waves excited by a microseism source have much lower amplitude and inconsistent shape com-
 191 pared to a repeating impulsive isolated noise sources (Fig. 3) due to decreased correlation of the source term with
 itself throughout time.

192 We repeat the numerical simulation above (Fig. 5) with $P(\theta, \phi)$ as the source term for both boundary and iso-
 193 lated noise sources (Fig. 7). Both contributions to the correlation wavefield are scaled to have similar amplitudes.
 194 A secondary microseism source produces repeating direct waves in correlation wavefields (Fig. 7b), similar to the

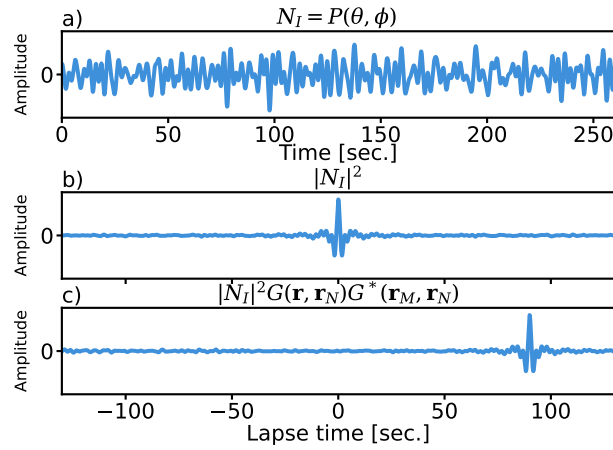


Figure 6 Contribution to the correlation wavefield by a continuously acting isolated noise source. a) Source term for a secondary microseism source, if all harmonics between 0.1 and 0.3 Hz are excited with a uniformly random phase $\Phi_i \in [0, 2\pi)$ and equal amplitude $A = 1$ (eq. 4). b) Auto-correlation of the source term $|N_I|^2$. c) Convolution of $|N_I|^2$ with the same Green's function cross-correlation as in Figure 3c, i.e., the second term of the correlation wavefield (eq. 2), with a main arrival and low-amplitude, repeating direct waves throughout the coda.

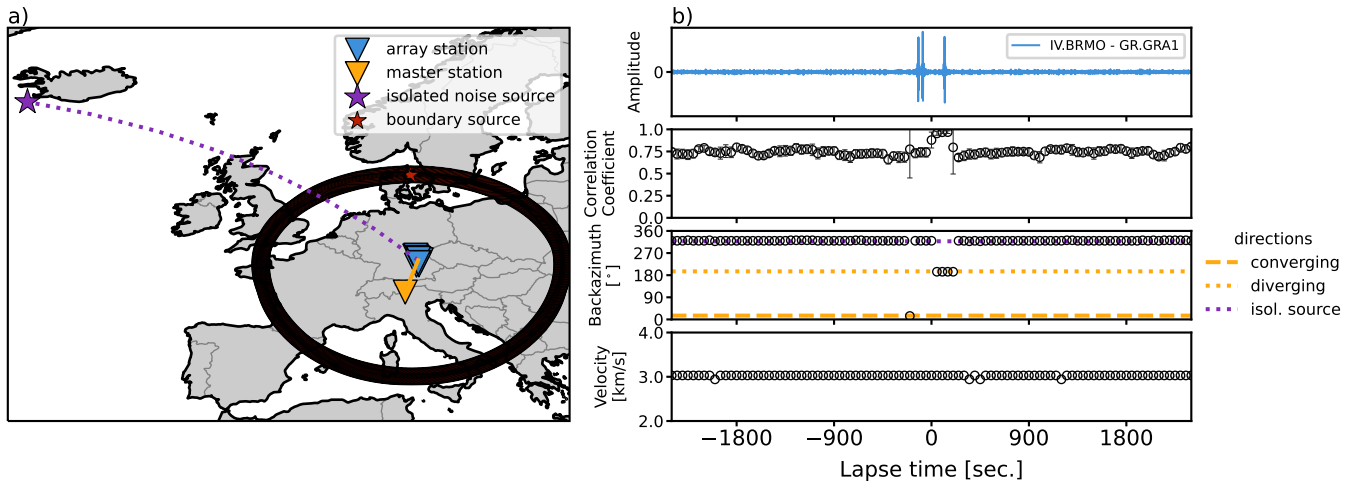


Figure 7 Same as Figure 5 but for secondary microseism source terms for both boundary and isolated sources. Both contributions to the correlation wavefield are scaled to have similar amplitudes. Distinct main arrival (the "spurious" arrival) of the isolated noise source at ~ -100 sec. lapse time. For this arrival and throughout the coda, direct waves from the isolated source are detected as most coherent.

195 regularly repeating source (Fig. 5). Near the main arrival of the isolated source (at ~ -100 sec., after the acausal
 196 arrival due to boundary sources) and throughout the coda, repeating direct waves from the isolated noise source lo-
 197 cation are detected as most coherent. Distinct main arrivals (the "spurious" arrival) have been observed for localised
 198 microseism sources before (Zeng and Ni, 2010; Retailleau et al., 2017). These main arrivals must arrive in-between
 199 the acausal and causal arrivals of the boundary source contribution (Schippkus et al., 2022). In this study, we do
 200 not observe a particularly clear main arrival on field data (Figs. 1, 2). Still, the coda of the field data correlation
 201 wavefields appears to be dominated by repeating waves from isolated noise sources. Correlation coefficients of the
 202 synthetic correlation functions with the beams for each window reach ~ 1 for the main causal arrival, and ~ 0.75
 203 for the acausal arrival due to interference with the isolated source arrival (Fig. 7b). Throughout the coda, correlation
 204 coefficients do not exceed 0.75 significantly, because continuously acting boundary sources also induce a repeating
 205 contribution in the correlation wavefield. In other words, the best beam does not represent the correlation functions

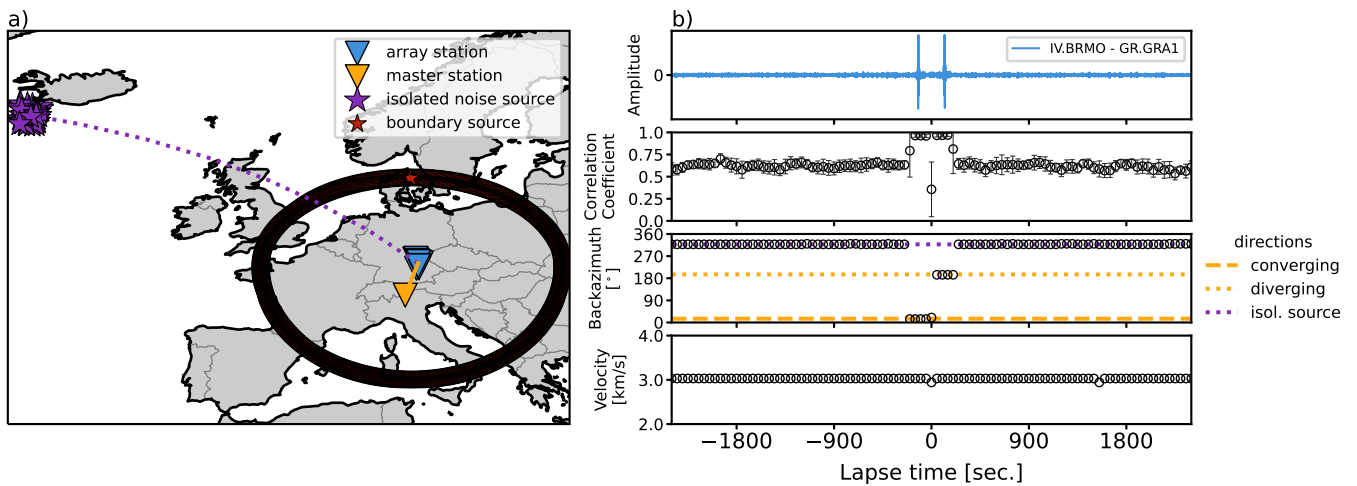


Figure 8 Same as Figure 7 but for a cluster of isolated sources. Amplitudes of the summed isolated noise source contribution is scaled to 1/10 of the boundary source contribution. No distinct spurious arrival but coda still dominated by repeating direct waves from the isolated noise source cluster.

entirely, even under the ideal conditions considered here, i.e., no heterogeneous structure, no dispersion, and no scattering.

To account for the fact we do not observe a distinct main arrival due to an isolated noise source in our field data correlations and to approximate a more realistic scenario by considering an extended source region, we place a cluster of 50 isolated noise sources Southwest of Iceland, each with a random realisation of the source term $P(\theta, \phi)$ and repeat the computations (Fig. 8). The wavefield contributions of those isolated noise sources, where each isolated source produces an additional term in equation (2), interfere to mask the main arrival (Fig. 8b). The amplitudes of the summed isolated noise source cluster contribution is scaled to 1/10 of the boundary source contribution. Beamforming correlation functions again detects the converging and diverging part of the boundary source contribution, as well as the isolated noise source cluster as dominant throughout the coda (Fig. 8b). Correlation coefficients with the beams stabilise at ~ 0.65 in the coda, and are lower than for the case of a single source (Fig. 7b).

Finally, we place a second cluster of 50 isolated noise sources Northwest of the Iberian Peninsula (Fig. 9a) to account for the observation that within the range of directions toward the Northern Atlantic, two distinct directions appear to dominate (Figs. 1, 2). Both clusters of isolated noise sources are treated separately and their combined amplitudes are again scaled to 1/10 of the boundary source contribution. Beamforming detects either one of the clusters as dominant, seemingly randomly throughout lapse time (Fig. 9b). Mean correlation coefficients with the beams are ~ 0.55 throughout the coda. This numerical simulation produces beamforming results closely resembling the measurements on field data correlation functions (Figs. 1, 2) and confirms that clusters of isolated noise sources produce repeating direct waves.

5 Discussion

In this study, we observe repeating direct waves propagating from isolated noise sources in the coda of correlation functions. We reproduce the observations by numerical modelling of continuously acting isolated sources.

The most significant question our analysis raises is: are repeating direct waves from isolated noise sources more dominant than multiply scattered waves, originating from the master station, also for individual correlation func-

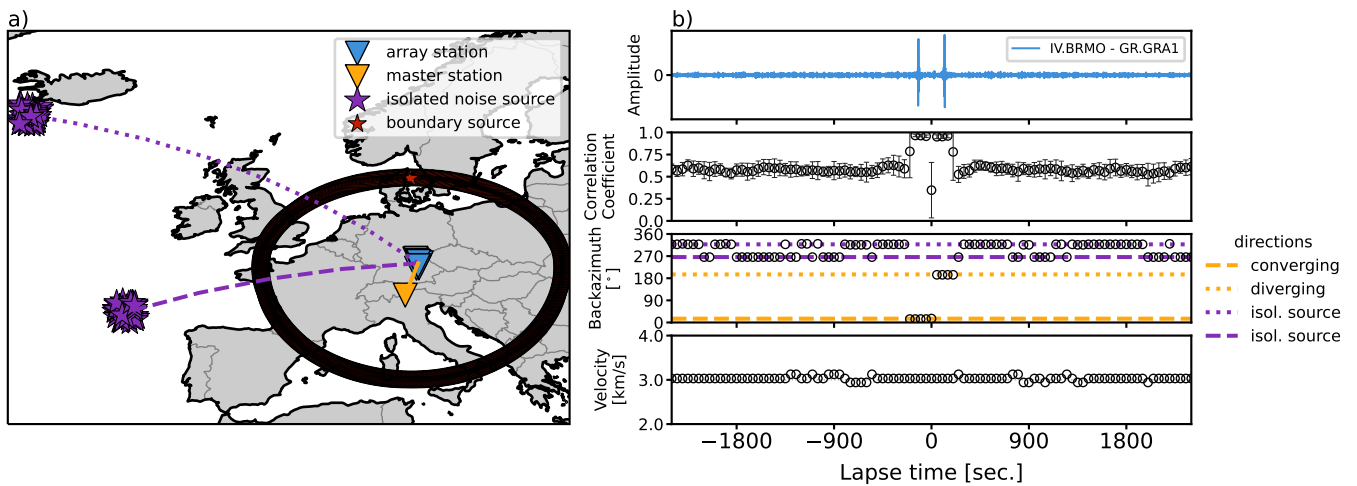


Figure 9 Same as Figure 8 but for two clusters of isolated noise sources. The additional cluster is placed Northwest of the Iberian Peninsula. The backazimuth to that cluster is indicated by a purple dashed line (a & b, third panel). Amplitudes of the isolated noise source contribution is scaled to 1/10 of the boundary source contribution. No distinct spurious arrival. Beamforming detects either of the two clusters at a given lapse time in the coda.

230 tions? If they did, our observations would have far-reaching implications. Beamforming, however, only shows that
 231 the contribution by isolated noise sources is more coherent across an array of stations (Figs. 1, 2). It is not surprising
 232 that multiply scattered waves can be incoherent across an array. To address this aspect, we compute correlation coef-
 233 ficients of all correlation functions with the beam in each beamforming window. These reach 0.75 to 0.9 (never 1) for
 234 the expected stronger, coherent acausal arrival on field data correlations (Figs. 1, 2), which indicates that not all fac-
 235 tors are accounted for during beamforming, namely heterogeneous structure, scattering, elastic wave propagation,
 236 and additional isolated sources. Still, these correlation coefficients provide a benchmark of what can be expected for
 237 the most coherent part of the correlation wavefield. In our numerical simulations, correlation coefficients are ~ 1
 238 for the main arrivals without the interference of distinct spurious arrivals (Figs. 5, 7, 8, 9). Throughout the coda, we
 239 observe that correlation coefficients remain nearly constant for both the field data examples (~ 0.4 , Figs. 1, 2) and
 240 the numerical simulations, decreasing with increasing complexity of the original wavefield from one isolated noise
 241 source (~ 0.75 , Fig. 7), to a cluster of sources (~ 0.65 , Fig. 8), to two clusters (~ 0.55 , Fig. 9). Without taking into ac-
 242 count the additional factors mentioned above (scattering, heterogeneous structure, or elastic waves), we reproduce
 243 a match between the modelled correlation functions and beams, comparable to the field data results. It is therefore
 244 reasonable to assume that the coda is not dominated by scattered waves, at least for absolute lapse times larger than
 245 a few hundred seconds.

246 At lapse times close to the direct arrivals from the master station (up to a few hundred seconds), correlation co-
 247 efficients are higher than for the later coda and a transition to the stable regime observed in the later coda appears
 248 to manifest (Figs. 1, 2). In the early coda, scattered waves are likely dominant and thus also coherent in the correla-
 249 tion wavefield, although question arise about the degree of scattering. The distinction between early coda and late
 250 coda arises, because amplitudes of the two correlation wavefield contributions decay for different reasons. Multiply
 251 scattered waves originating from the master station decay due to attenuation during wave propagation, whereas re-
 252 peating direct waves from isolated noise sources decay only due to correlation of the source term with itself through
 253 time (Figs. 3,6). As demonstrated above, even under ideal circumstances, amplitudes of repeating direct waves in

254 correlation functions decay due to the finite length of the source and signal considered (Fig. 3).

255 In the later coda (absolute lapse times larger than a few hundred seconds), the commonly held assumption that the
256 coda of a correlation wavefield is comprised dominantly, or even exclusively, of multiply scattered waves appears to be
257 false. The beams pointing towards isolated noise sources represent a significant fraction of the correlation wavefield
258 coda (Figs. 1, 2). Instead of spatially sampling the medium in a statistical manner (Margerin et al., 2016), the coda, and
259 thus measured velocity changes, may be dominantly sensitive to the path from the isolated noise source to the array
260 station. Note that repeating direct waves repeatedly travel the same path. A similar effect occurs in the presence of a
261 strong nearby scatterer (van Dinther et al., 2021). As the multiply scattered part of the correlation wavefield reaches
262 the strong scatterer, spatial sensitivity focuses along the path between stations and scatterer. In other words, the
263 scatterer "emits" a direct wave, induced by the master station, that is recorded in the coda of the correlation function.
264 This principle is similar to our considerations here, with the major difference that, in the modelling of van Dinther
265 et al. (2021), the direct wave propagating from the scatterer originates from the master station. For isolated noise
266 sources, direct waves originate from the source. The master station has no impact on the isolated source contribution
267 to the correlation wavefield, as long as it coherently records the same isolated noise sources as the array stations, as
268 the two field data examples suggest (Figs. 1, 2). We have no reason to suspect a strong scatterer to the West of the
269 Gräfenberg array that could explain our measurements. Instead, our measurements are consistent with repeating
270 direct waves from isolated noise sources, and reproduced by modelling without considering any scatterers. This
271 means that different station pairs do not lead to different spatial sensitivity when recording such repeating direct
272 waves. In some contexts, this may be advantageous by allowing repeated measurement of a repeating or continuous
273 isolated source by considering multiple master stations. In the context of seismic monitoring of relative velocity
274 variations, the impact of such sources has to be carefully considered.

275 The presence of repeating direct waves in the very late coda (30 minutes and more) furthermore challenges the
276 common assumption that the very late coda of correlation wavefields is dominated by instrument noise and contains
277 no useful signal. The very late coda is commonly used as a noise window for the estimation of signal-to-noise ratios
278 of correlation functions, also for coda windows. We show that the very late coda does instead contain useful infor-
279 mation, because repeating direct waves from isolated noise sources are still detected by beamforming (Figs. 1, 2).
280 This also suggests amplitudes decay only slowly due to low correlation of the isolated source with itself over time
281 (compared to Fig. 3), at least for the correlation wavefields investigated here, which were stacked over two years.

282 The early coda of correlation wavefields likely contains a significant contribution of scattered waves, as well as
283 direct repeating waves from isolated noise sources. This suggests great care should be taken in measuring velocity
284 variations and attributing them spatially also for the early coda. Common strategies to measure velocity variations,
285 e.g., the stretching method (Lobkis and Weaver, 2003), assume that absolute timing delays increase with lapse time,
286 because the seismic waves spent more time in the changed medium. For the contribution by repeating direct waves,
287 stretching should not occur since absolute time delays are likely constant throughout the coda, as long as the isolated
288 source does not move. A strategy that involves estimating the degree of stretching throughout the coda may give in-
289 sight into the dominant regime (scattered waves vs. repeating waves) and whether the measurement approach is
290 applicable. A different strategy to discriminate the correlation wavefield contributions may be to include measure-

291 ments of wavefield gradients, which allow to separate the seismic wavefield using only single stations [Sollberger et al.](#)
 292 (2023).

293 Further questions arise about the temporal sensitivity of measured velocity variations. When considering scat-
 294 tered waves in the coda, velocity variation measurements are usually attributed to the entire time window used for
 295 correlation, e.g, a single measurement that represents an entire day. Repeating direct waves from isolated noise
 296 sources should in principle allow to improve temporal resolution, because arrivals at different lapse times likely
 297 have different temporal sensitivity in "real" time. However, it is not immediately obvious what time exactly a specific
 298 repeated arrival is sensitive to. This is a target for future studies.

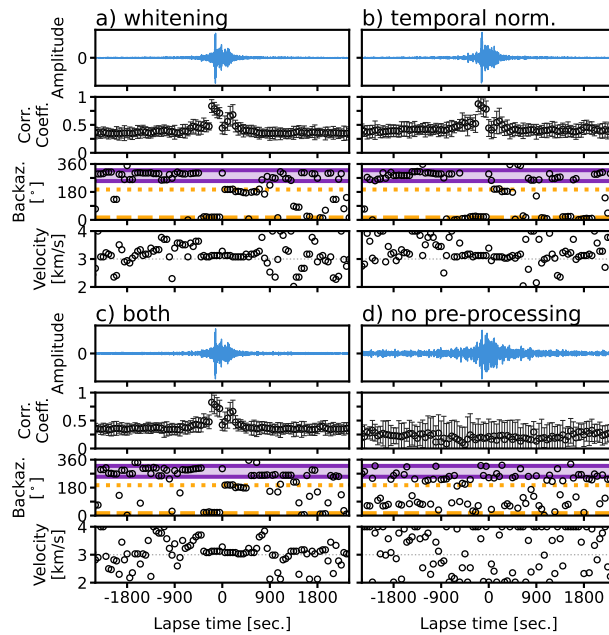


Figure 10 Impact of pre-processing scheme on the detection of repeating direct waves for master station IV.BRMO. a) Same as Figure 1b. b) Sample correlation function and beamforming result, if only temporal normalisation is applied. c) Results when both whitening and temporal normalisation are applied. d) Results when neither pre-processing is applied.

299 Pre-processing of seismic records before cross-correlation plays an important role when investigating cross correla-
 300 tions of ambient seismic noise. We apply spectral whitening, a commonly adopted pre-processing strategy ([Bensen](#)
 301 [et al., 2007](#)). Spectral whitening is the normalisation of the amplitude spectrum before cross-correlation, often with
 302 a water level or smoothed spectrum to avoid introducing artefacts. Whitening is often successful in suppressing the
 303 impact of near-monochromatic signals, e.g., in the context of the 26 sec. microseism in the Gulf of Guinea ([Bensen](#)
 304 [et al., 2007](#)) or wind turbine noise ([Schippkus et al., 2022](#)). On the other hand, whitening will also emphasise sig-
 305 nals with relatively low amplitude in the original data. To confirm that our interpretation of the results above is
 306 not significantly biased by the processing strategy, we repeat the measurements for master station IV.BRMO (Fig.
 307 1) with temporal normalisation, both whitening and temporal normalisation, and neither pre-processing (Fig. 10).
 308 Temporal normalisation (running window average) is performed in a 5 sec. moving window. As long as any pro-
 309 cessing to stabilise the correlation functions is applied (Fig. 10a-c), the fundamental observation of repeating direct
 310 waves remains. Slight differences emerge in the correlation functions themselves, and also which direction direc-
 311 tion and velocity are detected at a given lapse time. Temporal normalisation is commonly applied in studies that
 312 measure relative velocity variations, often in its most extreme version one-bit normalisation. Here we demonstrate

313 that common pre-processing schemes produce correlation functions with repeating direct waves. Without any pro-
314 cessing, however, results become unstable and beamforming neither detects stable directions of arrival nor gives
315 consistent phase velocity estimates (Fig. 10d). Correlation functions are more stable after such pre-processing, as is
316 commonly observed, because these approaches (in addition to addressing some data glitches) reduce the impact of
317 certain isolated noise sources on the recorded wavefield, in particular from transient high-amplitude sources (e.g.,
318 earthquakes) and continuous near-monochromatic sources (e.g., machinery). The sources that remain as dominant,
319 after this pre-processing is applied, are continuously acting broadband sources (e.g., ocean microseisms) as is con-
320 firmed by beamforming (Figs. 1 & 2).

321 Machinery- or traffic-based monitoring of velocity variations is likely similarly affected by the findings in this
322 study. Rotating machinery, such as generators in wind turbines (Friedrich et al., 2018; Schippkus et al., 2020; Nagel
323 et al., 2021), likely have source terms that are significantly correlated throughout time due to their mechanism, with
324 higher correlation than ocean microseisms. These sources could produce repeating direct waves with high ampli-
325 tude. Traffic, e.g., trains repeatedly passing the same spot, resembles repeatedly acting noise sources (as in Fig. 3),
326 although with more complex wavelets. In case of traffic at a regular interval, e.g., trains on a schedule, the late coda
327 of the correlation wavefield could allow to extract their signature reliably. Recently, approaches that identify and se-
328 lect appropriate time windows to use for cross-correlation and subsequent velocity monitoring have emerged (e.g.,
329 Yates et al., 2022; Sheng et al., 2023). These approaches are motivated by the realisation that correlation wavefields
330 can be highly complex and depend significantly on the presence of isolated noise sources, similar to this study. Still,
331 our findings also have impact on these strategies. In time windows where an isolated noise source is known to be
332 particularly active, repeating direct waves may still emerge and coincide with the coda of that source, depending
333 on the source signature and length of time window considered for cross-correlation. Further investigations on this
334 aspect may help improve the accuracy of detected velocity changes in time and space.

335 **6 Conclusion**

336 Continuously acting isolated noise sources generate repeating direct waves that may dominate the coda of correlation
337 wavefields, as observed on field data correlations (Figs. 1, 2) and reproduced by numerical simulations (Figs. 3-
338 9). In the simulations, we start from the established concept of an isolated noise source (Schippkus et al., 2022)
339 that repeatedly excites a wavelet to illustrate the fundamental principle of how repeated direct waves emerge in
340 correlation functions (Figs. 3, 5). To better reproduce the measurements on field data correlations, we model an
341 isolated secondary microseism source, starting with one source (Fig. 7), which shows a distinct main arrival of that
342 source (the "spurious arrival") that is not always observed clearly on field data correlations. With a cluster of isolated
343 noise sources, mimicking an extended source region, this main arrival disappears due to interference between the
344 sources (Fig. 8). Finally, we model two clusters to show that either may be detected at a given lapse time (Fig. 9),
345 reliably reproducing the observations on our field data correlation wavefields (Figs. 1, 2). Throughout our modelling,
346 we keep the numerical setup as simple as possible to emphasise the impact of only the isolated noise sources, i.e., we
347 exclude any influence due to heterogeneous Earth structure, any elastic wave propagation effects such as multiple
348 wave types or conversion between them, and importantly do not include any scattering.

Our results suggest that the coda of correlation wavefields should not be assumed to be mainly comprised of scattered waves, which originated from the master station. Instead, repeating direct waves from isolated noise sources may dominate. There is likely a transition in dominating regime from scattered waves (in the early coda) to repeating direct waves (in the late coda). This occurs, because amplitudes of scattered waves decay due to attenuation, whereas repeating direct waves decay slower only due to the auto-correlation of the source term throughout time. This has implications for ambient noise correlation based monitoring applications, commonly assuming multiply scattered waves, and raises questions about the validity of such measurements, in particular about the spatial sensitivity.

This study also opens up new opportunities for future research. In the presence of a continuously acting isolated noise source, the very late coda of correlation wavefields retains the source signature and is not dominated by instrument noise. This in principle allows to extract seismic waves repeatedly propagating along the same path, undisturbed by other contributions, which may be an attractive target for monitoring applications. The spatial distribution of isolated noise sources, however, severely limits the spatial sensitivity of the very late correlation wavefield coda.

Data Availability and Resources

This manuscript is fully reproducible. All computed correlation functions and code necessary to produce all figures are hosted on Github and Zenodo (Schippkus, 2023). Seismograms used in this study to compute correlation functions are provided by the network operators of the German Regional Seismic Network (GR, Federal Institute for Geosciences and Natural Resources, 1976), Polish Seismological Network (PL, Polish Academy of Sciences (PAN) Polskiej Akademii Nauk, 1990), and Italian National Seismic Network (IV, Istituto Nazionale di Geofisica e Vulcanologia (INGV), 2005). We rely on open-source software for our computations and visualisations (Hunter, 2007; Met Office, 2010; Krischer et al., 2015; Harris et al., 2020; Virtanen et al., 2020). Color sequences are designed to be accessible (Petroff, 2021).

Acknowledgements

The authors acknowledge funding provided by the Emmy Noether program (HA7019/1-1) of the German Research Foundation (DFG). The authors acknowledge funding provided by the European Union's Horizon 2020 research and innovation programme under the Marie Skłodowska-Curie grant agreement No. 955515 (SPIN ITN).

References

- Bensen, G. D., Ritzwoller, M. H., Barmin, M. P., Levshin, A. L., Lin, F., Moschetti, M. P., Shapiro, N. M., and Yang, Y. Processing Seismic Ambient Noise Data to Obtain Reliable Broad-Band Surface Wave Dispersion Measurements. *Geophysical Journal International*, 169(3):1239–1260, June 2007. doi: 10.1111/j.1365-246X.2007.03374.x.
- Chevrot, S., Sylvander, M., Benahmed, S., Ponsolles, C., Lefèvre, J. M., and Paradis, D. Source Locations of Secondary Microseisms in Western Europe: Evidence for Both Coastal and Pelagic Sources. *Journal of Geophysical Research: Solid Earth*, 112(B11), Nov. 2007. doi: 10.1029/2007JB005059.
- Federal Institute for Geosciences and Natural Resources. German Regional Seismic Network (GRSN), 1976.

- 383 Friedrich, A., Krüger, F., Klinge, K., and 1998. Ocean-Generated Microseismic Noise Located with the Gräfenberg Array. *Journal of Seismology*,
384 2:47–64, 1998. doi: 10.1023/A:1009788904007.
- 385 Friedrich, T., Zieger, T., Forbriger, T., and Ritter, J. R. R. Locating Wind Farms by Seismic Interferometry and Migration. *Journal of Seismology*,
386 22(6):1469–1483, Nov. 2018. doi: 10.1007/s10950-018-9779-0.
- 387 Gouédard, P., Stehly, L., Brenguier, F., Campillo, M., Colin de Verdière, Y., Larose, E., Margerin, L., Roux, P., Sánchez-Sesma, F. J., Shapiro,
388 N. M., and Weaver, R. L. Cross-Correlation of Random Fields: Mathematical Approach and Applications. *Geophysical Prospecting*, 56(3):
389 375–393, 2008. doi: 10.1111/j.1365-2478.2007.00684.x.
- 390 Gualtieri, L., Bachmann, E., Simons, F. J., and Tromp, J. The Origin of Secondary Microseism Love Waves. *Proceedings of the National*
391 *Academy of Sciences of the United States of America*, 117(47):29504–29511, Nov. 2020. doi: 10.1073/pnas.2013806117.
- 392 Hadziioannou, C., Larose, E., Coutant, O., Roux, P., and Campillo, M. Stability of Monitoring Weak Changes in Multiply Scattering Media
393 with Ambient Noise Correlation: Laboratory Experiments. *The Journal of the Acoustical Society of America*, 125(6):3688–3695, June 2009.
394 doi: 10.1121/1.3125345.
- 395 Harris, C. R., Millman, K. J., van der Walt, S. J., Gommers, R., Virtanen, P., Cournapeau, D., Wieser, E., Taylor, J., Berg, S., Smith, N. J., Kern,
396 R., Picus, M., Hoyer, S., van Kerkwijk, M. H., Brett, M., Haldane, A., del Río, J. F., Wiebe, M., Peterson, P., Gérard-Marchant, P., Sheppard, K.,
397 Reddy, T., Weckesser, W., Abbasi, H., Gohlke, C., and Oliphant, T. E. Array Programming with NumPy. *Nature*, 585(7825):357–362, Sept.
398 2020. doi: 10.1038/s41586-020-2649-2.
- 399 Hunter, J. D. Matplotlib: A 2D Graphics Environment. *Computing in Science & Engineering*, 9(3):90–95, 2007. doi: 10.1109/MCSE.2007.55.
- 400 Istituto Nazionale di Geofisica e Vulcanologia (INGV). Rete Sismica Nazionale (RSN), 2005.
- 401 Juretzek, C. and Hadziioannou, C. Where Do Ocean Microseisms Come from? A Study of Love-to-Rayleigh Wave Ratios. *Journal of Geophys-*
402 *ical Research: Solid Earth*, 121(9):6741–6756, Sept. 2016. doi: 10.1002/2016JB013017.
- 403 Krischer, L., Megies, T., Barsch, R., Beyreuther, M., Lecocq, T., Caudron, C., and Wassermann, J. ObsPy: A Bridge for Seismology into the
404 Scientific Python Ecosystem. *Computational Science & Discovery*, 8(014003), Jan. 2015. doi: 10.1088/1749-4699/8/1/014003.
- 405 Lobkis, O. I. and Weaver, R. L. Coda-Wave Interferometry in Finite Solids: Recovery of P-to-S Conversion Rates in an Elastodynamic Billiard.
406 *Physical Review Letters*, 90(25):254302, June 2003. doi: 10.1103/PhysRevLett.90.254302.
- 407 Lu, Y., Stehly, L., Paul, A., and the AlpArray Working Group. High-Resolution Surface Wave Tomography of the European Crust and Uppermost
408 Mantle from Ambient Seismic Noise. *Geophysical Journal International*, 214(2):1136–1150, May 2018. doi: 10.1093/gji/ggy188.
- 409 Mao, S., Lecointre, A., van der Hilst, R. D., and Campillo, M. Space-Time Monitoring of Groundwater Fluctuations with Passive Seismic
410 Interferometry. *Nature Communications*, 13(1):4643, Aug. 2022. doi: 10.1038/s41467-022-32194-3.
- 411 Margerin, L., Planès, T., Mayor, J., and Calvet, M. Sensitivity Kernels for Coda-Wave Interferometry and Scattering Tomography: Theory and
412 Numerical Evaluation in Two-Dimensional Anisotropically Scattering Media. *Geophysical Journal International*, 204(1):650–666, Jan.
413 2016. doi: 10.1093/gji/ggv470.
- 414 Met Office. *Cartopy: A Cartographic Python Library with a Matplotlib Interface*. Exeter, Devon, 2010.
- 415 Nagel, S., Zieger, T., Luhmann, B., Knödel, P., Ritter, J., and Ummerhofer, T. Ground Motions Induced by Wind Turbines. *Civil Engineering*
416 *Design*, 3(3):73–86, 2021. doi: 10.1002/cend.202100015.
- 417 Obermann, A., Froment, B., Campillo, M., Larose, E., Planès, T., Valette, B., Chen, J. H., and Liu, Q. Y. Seismic Noise Correlations to Image
418 Structural and Mechanical Changes Associated with the Mw 7.9 2008 Wenchuan Earthquake. *Journal of Geophysical Research: Solid*
419 *Earth*, 119(4):3155–3168, Apr. 2014. doi: 10.1002/2013JB010932.
- 420 Petroff, M. A. Accessible Color Sequences for Data Visualization. July 2021. doi: 10.48550/arXiv.2107.02270.

- 421 Planès, T., Larose, E., Margerin, L., Rossetto, V., and Sens-Schönfelder, C. Decorrelation and Phase-Shift of Coda Waves Induced by Lo-
422 cal Changes: Multiple Scattering Approach and Numerical Validation. *Waves in Random and Complex Media*, 24(2):99–125, Apr. 2014.
423 doi: 10.1080/17455030.2014.880821.
- 424 Polish Academy of Sciences (PAN) Polskiej Akademii Nauk. Polish Seismological Network, 1990.
- 425 Retailleau, L., Boué, P., Stehly, L., and Campillo, M. Locating Microseism Sources Using Spurious Arrivals in Intercontinental Noise Correla-
426 tions. *Journal of Geophysical Research: Solid Earth*, 122(10):8107–8120, 2017. doi: 10.1002/2017JB014593.
- 427 Rost, S. and Thomas, C. Array Seismology: Methods and Applications. *Reviews of Geophysics*, 40(3):2–1–2–27, 2002.
428 doi: 10.1029/2000RG000100.
- 429 Schippkus, S. Schipp/Repeating_direct_waves: V0.1 - Pre-Print Prep. Feb. 2023. doi: 10.5281/zenodo.7643286.
- 430 Schippkus, S., Zigone, D., Bokelmann, G. H. R., and the AlpArray Working Group. Ambient-Noise Tomography of the Wider Vienna Basin
431 Region. *Geophysical Journal International*, 215(1):102–117, June 2018. doi: 10.1093/gji/ggy259.
- 432 Schippkus, S., Garden, M., and Bokelmann, G. Characteristics of the Ambient Seismic Field on a Large-N Seismic Array in the Vienna Basin.
433 *Seismological Research Letters*, 91(5):2803–2816, July 2020. doi: 10.1785/0220200153.
- 434 Schippkus, S., Snieder, R., and Hadziioannou, C. Seismic Interferometry in the Presence of an Isolated Noise Source. *Seismica*, 1(1), Dec.
435 2022. doi: 10.26443/seismica.v1i1.195.
- 436 Sens-Schönfelder, C. and Larose, E. Lunar Noise Correlation, Imaging and Monitoring. *Earthquake Science*, 23(5):519–530, Oct. 2010.
437 doi: 10.1007/s11589-010-0750-6.
- 438 Sheng, Y., Mordret, A., Brenguier, F., Boué, P., Vernon, F., Takeda, T., Aoki, Y., Taira, T., and Ben-Zion, Y. Seeking Repeating Anthropogenic
439 Seismic Sources: Implications for Seismic Velocity Monitoring at Fault Zones. *Journal of Geophysical Research: Solid Earth*, 128(1), Jan.
440 2023. doi: 10.1029/2022JB024725.
- 441 Snieder, R., Wapenaar, K., and Larner, K. Spurious Multiples in Seismic Interferometry of Primaries. *GEOPHYSICS*, 71(4):SI111–SI124, July
442 2006. doi: 10.1190/1.2211507.
- 443 Soergel, D., Pedersen, H. A., Bodin, T., Paul, A., Stehly, L., AlpArray Working Group, Hetényi, G., Abreu, R., Allegretti, I., Apoloner, M.-T., Aubert,
444 C., Bes De Berc, M., Bokelmann, G., Brunel, D., Capello, M., Cărman, M., Cavaliere, A., Chèze, J., Chiarabba, C., Clinton, J., Cougoulat, G.,
445 Crawford, W., Cristiano, L., Czifra, T., D’Alema, E., Danesi, S., Daniel, R., Dasović, I., Deschamps, A., Dessa, J.-X., Doubre, C., and Egdorf, S.
446 Bayesian Analysis of Azimuthal Anisotropy in the Alpine Lithosphere from Beamforming of Ambient Noise Cross-Correlations. *Geophys-
447 ical Journal International*, 232(1):429–450, Sept. 2022. doi: 10.1093/gji/ggac349.
- 448 Sollberger, D., Bradley, N., Edme, P., and Robertsson, J. O. A. Efficient Wave Type Fingerprinting and Filtering by Six-Component Polarization
449 Analysis. *Geophysical Journal International*, 234(1):25–39, Feb. 2023. doi: 10.1093/gji/ggad071.
- 450 van Dintner, C., Margerin, L., and Campillo, M. Implications of Laterally Varying Scattering Properties for Subsurface Monitoring With Coda
451 Wave Sensitivity Kernels: Application to Volcanic and Fault Zone Setting. *Journal of Geophysical Research: Solid Earth*, 126(12), Dec.
452 2021. doi: 10.1029/2021JB022554.
- 453 Virtanen, P., Gommers, R., Oliphant, T. E., Haberland, M., Reddy, T., Cournapeau, D., Burovski, E., Peterson, P., Weckesser, W., Bright, J., van
454 der Walt, S. J., Brett, M., Wilson, J., Millman, K. J., Mayorov, N., Nelson, A. R. J., Jones, E., Kern, R., Larson, E., Carey, C. J., Polat, İ., Feng,
455 Y., Moore, E. W., VanderPlas, J., Laxalde, D., Perktold, J., Cimrman, R., Henriksen, I., Quintero, E. A., Harris, C. R., Archibald, A. M., Ribeiro,
456 A. H., Pedregosa, F., van Mulbregt, P., and SciPy 1.0 Contributors. SciPy 1.0: Fundamental Algorithms for Scientific Computing in Python.
457 *Nature Methods*, 17:261–272, 2020. doi: 10.1038/s41592-019-0686-2.
- 458 Wapenaar, K., Fokkema, J., and Snieder, R. Retrieving the Green’s Function in an Open System by Cross Correlation: A Comparison of

- 459 Approaches (L). *The Journal of the Acoustical Society of America*, 118(5):2783–2786, Nov. 2005. doi: 10.1121/1.2046847.
- 460 Wegler, U. and Sens-Schönfelder, C. Fault Zone Monitoring with Passive Image Interferometry. *Geophysical Journal International*, 168(3):
461 1029–1033, Mar. 2007. doi: 10.1111/j.1365-246X.2006.03284.x.
- 462 Yates, A., Caudron, C., Lesage, P., Mordret, A., Lecocq, T., and Soubestre, J. Assessing Similarity in Continuous Seismic Cross-Correlation
463 Functions Using Hierarchical Clustering: Application to Ruapehu and Piton de La Fournaise Volcanoes. *Geophysical Journal International*,
464 233(1):472–489, Nov. 2022. doi: 10.1093/gji/ggac469.
- 465 Zeng, X. and Ni, S. A Persistent Localized Microseismic Source near the Kyushu Island, Japan. *Geophysical Research Letters*, 37(24), 2010.
466 doi: 10.1029/2010GL045774.